

INTERACTION OF LASER RADIATION WITH MATTER. LASER PLASMA https://doi.org/10.1070/QEL17389

Effect of postgrowth processing technology and laser radiation parameters at wavelengths of 2091 and 1064 nm on the laser-induced damage threshold in $ZnGeP_2$ single crystal

N.N. Yudin, O.L. Antipov, A.I. Gribenyukov, I.D. Eranov, S.N. Podzyvalov, M.M. Zinoviev, L.A. Voronin, E.V. Zhuravleva, M.P. Zykova

Abstract. **We report a study of the effect of postgrowth treatment of $ZnGeP_2$ single crystals (low-temperature annealing, irradiation with fast electrons, polishing of working surfaces) and the conditions of exposure to repetitively pulsed laser radiation [wavelength (2091 or 1064 nm), pulse repetition rate, beam diameter, exposure time, sample temperature] on the laser-induced damage threshold (LIDT) of the surfaces of these crystals. It is found that thermal annealing of $ZnGeP_2$ single crystals and their irradiation with a flux of fast electrons, which increase the LIDT at a wavelength of λ = 1064 nm, do not lead to a change in this threshold at λ = 2091 nm. It is shown that $ZnGeP_2$ elements with lower optical losses in the spectral range 0.7–2.5 μm have a higher LIDT at λ = 2091 nm both immediately after fabrication and after postgrowth processing. An increase in the threshold energy density of laser radiation by a factor of 1.5–3 at λ = 2091 nm is revealed with a decrease in the crystal temperature from zero to –60 °C. The fact of reversible photodarkening of the propagation channel of laser radiation in $ZnGeP_2$ in the predamage region of parameters is established by the method of digital holography.**

Keywords: *$ZnGeP_2$ single crystal, optical damage, postgrowth treatments, surface polishing, radiation of Ho^{3+}:YAG- and Nd^{3+}:YAG lasers.*

1. Introduction

Repetitively pulsed sources of high-power coherent mid-IR radiation are widely used in such areas as processing of (materials glass, ceramics, or semiconductors) [1, 2], atmospheric sounding for remote determination of the composition of substances and environmental monitoring [3–5] and also medicine, including diagnostics of diseases using gas analysis and resonance ablation of biological tissues [6, 7].

One of the most efficient solid-state sources of coherent radiation in the mid-IR range are optical parametric oscillators (OPOs). The most high-power OPOs in the 3500–5000 nm wavelength range are currently fabricated on the basis of nonlinear optical crystals $ZnGeP_2$ (ZGP) [8]. ZGP-based OPOs are capable of generating radiation with an average power of up to 100 W or an energy per pulse of up to 200 mJ with a pulse width of 20–40 ns and a pulse repetition rate from a few hertz to one hundred kilohertz [9–11]. Unfortunately, the reliable long-term operation of high-power ZGP-based OPOs is limited by optical damage (or laser damage) of this material. In this regard, the expansion of the practical use of high-power OPOs in the mid-IR range is associated with the need to reveal the physical mechanisms of laser damage. Although optical damage is a well-known effect, clarifying its mechanism is an independent task in each specific case [12, 13].

The problem of ZGP optical damage by laser radiation at wavelengths of 1064 and 2100 nm in the region of ~10 μm has been discussed in a number of papers [14–19]. It was reported, in particular, that the laser-induced damage threshold (LIDT) of the ZGP surface is related to the density of the pump radiation energy and is almost independent of the radiation intensity [14]. It was shown that improving the quality of polishing of working surfaces and reducing or completely removing the near-surface fractured layer leads to an increase in the LIDT [15]. In this case, the LIDT of a ZGP crystal with antireflection coatings at a wavelength of 2050 nm was ~2 J cm^{-2} at a pulse repetition rate $f \approx 10$ kHz [15], which is five times less than the previously measured damage threshold of the same crystal under the action of

N.N. Yudin Institute of Applied Physics, Russian Academy of Sciences, ul. Ulyanova 46, 603950 Nizhny Novgorod, Russia; National Research Tomsk State University, prosp. Lenina 36, 634050 Tomsk, Russia; Zuev Institute of Atmospheric Optics, Siberian Branch, Russian Academy of Sciences, pl. Akad. Zueva 1, 634055 Tomsk, Russia; LLC 'Laboratory of Optical Crystals', ul. Vysotskogo 28, stroenie 7, 634040 Tomsk, Russia; e-mail: rach3@yandex.ru;
O.L. Antipov Institute of Applied Physics, Russian Academy of Sciences, ul. Ulyanova 46, 603950 Nizhny Novgorod, Russia; Lobachevsky State University of Nizhny Novgorod, prosp. Gagarina 23, 603950 Nizhny Novgorod, Russia;
A.I. Gribenyukov LLC 'Laboratory of Optical Crystals', ul. Vysotskogo 28, stroenie 7, 634040 Tomsk, Russia; Institute of Monitoring of Climatic and Ecological Systems, Siberian Branch, Russian Academy of Sciences, Akademicheskii prosp. 10/3, 634055 Tomsk, Russia;
I.D. Eranov Institute of Applied Physics, Russian Academy of Sciences, ul. Ulyanova 46, 603950 Nizhny Novgorod, Russia;
S.N. Podzyvalov Zuev Institute of Atmospheric Optics, Siberian Branch, Russian Academy of Sciences, pl. Akad. Zueva 1, 634055 Tomsk, Russia; LLC 'Laboratory of Optical Crystals', ul. Vysotskogo 28, stroenie 7, 634040 Tomsk, Russia;
M.M. Zinoviev National Research Tomsk State University, prosp. Lenina 36, 634050 Tomsk, Russia; Zuev Institute of Atmospheric Optics, Siberian Branch, Russian Academy of Sciences, pl. Akad. Zueva 1, 634055 Tomsk, Russia; LLC 'Laboratory of Optical Crystals', ul. Vysotskogo 28, stroenie 7, 634040 Tomsk, Russia;
L.A. Voronin Budker Institute of Nuclear Physics, Siberian Branch, Russian Academy of Sciences, prosp. Akad. Lavrent'eva 11, 630090 Novosibirsk, Russia;
E.V. Zhuravleva National Research Tomsk State University, prosp. Lenina 36, 634050 Tomsk, Russia;
M.P. Zykova Mendeleev Russian University of Chemical Technology, Miusskaya pl. 9, 125047 Moscow, Russia

Received 25 June 2020; revision received 27 January 2021
Kvantovaya Elektronika **51** (4) 306–316 (2021)
Translated by V.L. Derbov

radiation at $\lambda = 2$ μm and $f \approx 1$ Hz [14]. A significant difference was revealed in the LIDT values for the ZGP crystal at wavelengths of 1064 and 2100 nm [16]. Dynamic visualisation of the process of damage by laser radiation at $\lambda = 2100$ nm in the ZGP volume showed that an avalanche-like increase in temperature occurs in the forming track inside the nonlinear optical element [17]. The LIDT of ZGP elements at $\lambda = 9.55$ μm was determined from the intensity of the incident beam 142 MW cm^{-2} at a pulse width $\tau_p = 85$ ns and a pulse repetition rate $f = 1$ Hz [18], which corresponds to a pulse energy density of ~9.5 J cm^{-2}. The report in [19] about an increase in the ZGP damage threshold with decreasing pump pulse width '...testifies in favour of the thermal nature of damage for nanosecond pulses due to anomalous infrared absorption' [20, 21]. Thus, the large scatter of the LIDT values of the ZGP crystal and the differences in the interpretation of the results of previous studies show that the physical mechanism of laser damage and its dependence on the factors of technological processing and experimental parameters remain not fully understood.

The aim of this work is to clarify the influence of the parameters of postgrowth technological operations (low-temperature annealing, exposure to fast electrons, polishing of working surfaces) and the experimental conditions (pulse width and repetition rate, beam diameter, exposure time, element temperature) on the LIDT of the ZGP crystals surface under the action of a laser radiation at wavelengths of 2091 and 1064 nm.

2. Single crystal samples and the method of their postgrowth processing

To study optical damage, we used two different ZGP single crystals (I and II), from which nine samples were cut. Seven plates (samples 1–7) 30 mm in diameter and 3 mm thick were cut from crystal I parallel to the crystallographic plane (100), two other elements (samples 8 and 9) 6 × 6 × 20 mm in size were cut from crystal II at angles $\theta = 54.5°$ and $\varphi = 0$ relative to the optical axis. Both ZGP single crystals were grown by the Bridgman method in the vertical direction on an oriented seed as described in [22].

The previously synthesised material used for the growth of single crystals was examined for the presence of impurities. The concentrations of impurity chemical elements were determined by inductively coupled plasma mass spectrometry (NexION300D, PerkinElmer, USA) in preparations at the Department of Chemistry and Technology of Crystals of the Russian Chemical Technology University (Moscow). For analysis, a solid sample was dissolved in a mixture of high-purity mineral acids under microwave autoclaving conditions (SpeedWAVE FOUR, Berghoff, Germany) in PTFE autoclaves. The content of impurity elements (their concentration in the sample exceeded 10^{-8} wt%), shown in the histogram (Fig. 1), was the same in both studied ZGP single crystals.

Table 1. Results of X-ray diffraction analysis of the samples under study.

Sample	Lattice parameters/Å	CSR size/nm
1–6	$a = 5.468$ $c = 10.714$	35
7	$a = 5.471$ $c = 10.706$	88
8	$a = 5.461$ $c = 10.707$	35

Note: For all samples, only $ZnGeP_2$ phases with a concentration of 100 wt% were found; CSR is a coherent scattering region in which X-rays are scattered coherently and independently of other similar regions.

Before the start of the study, the phase composition of the samples was also determined using X-ray diffraction analysis. The study was carried out at a wavelength of 1.541862 Å on a Rigaku MiniFlex 600 X-ray diffractometer having an X-ray tube with a copper anode. The phase composition was analysed using the PDF 4$^+$ database and the POWDER CELL 2.4 full-profile analysis program. The survey was carried out in the range of angles 3–60° with a step of 0.02°. Samples for X-ray diffraction analysis were cut from single crystals I and II and ground to a powdery state. According to the results of X-ray structural analysis, no residual components of the synthesis – the second phases (Zn_3P_2, ZnP_2, GeP) – were revealed in all the samples under study (Table 1).

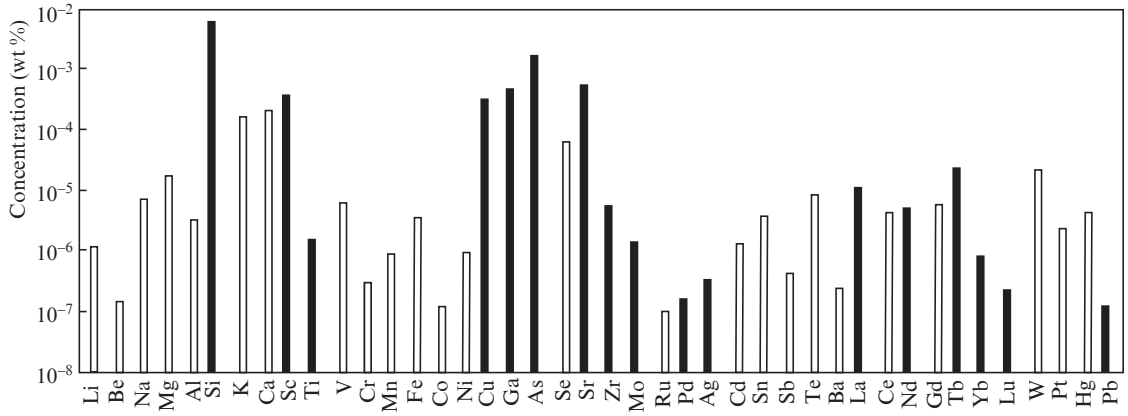

Figure 1. Impurity composition of ZGP crystals as determined by inductively coupled plasma mass spectrometry. White bars indicate the limit of determination of the content of impurity elements for a particular element (i.e., the concentration of impurities of a particular chemical element does not exceed the value corresponding to the height of the white bar), the height of the black bars corresponds to the mass fraction of the content of the impurity element, when the limit of determination is an order of magnitude less than the measured concentration of the chemical element.

With the help of a digital holographic camera DCH-1064 manufactured by LLC 'LOK' (Tomsk, Russia), holograms of the internal volume of all studied samples were obtained. To determine internal inhomogeneities and volumetric defects resulting from the presence of residual components of synthesis in the material [23], the obtained holographic images were reconstructed. The limiting resolution of the method was 3 μm (a detailed description of the digital holography technique, including that related to the visualisation of defects in $ZnGeP_2$, is given in [23–25]). In all the samples studied in this work, within the limits of the method resolution, no bulk defects were detected in the entire volume of the material (including the surface).

Some of the samples under study after growth were not subjected to thermal annealing and irradiation with a flow of fast electrons – technological operation A. Some of the samples after growth were subjected to thermal annealing at a temperature of 600 °C – technological operation B. Some of the samples after annealing were irradiated with a flow of fast electrons (with an energy of 5 MeV and a flux density of 2.2×10^{17} electrons cm^{-2}) – technological operation C.

The working surfaces of all the samples were processed on a 4-PD-200 polishing and finishing machine. Initial treatment consisted of polishing on a cambric polish using ACM 0.5/0 synthetic diamond powder (average grain size 270 nm). In this case, a fractured layer with a thickness of ~30 μm formed in the process of cutting the crystal into oriented plates and their preliminary grinding was removed, – polishing procedure D. Two samples (1 and 2) were not subjected to subsequent polishing, the rest were additionally polished on a cambric polishing pad using synthetic diamond powder ACM 0.25/0 – polishing procedure E. Next, the samples were polished on a resin polishing pad, also using ACM 0.25/0 – polishing procedure F. One of the polished working surfaces of samples 1–6 was coated with an antireflection coating to provide transmission over 98% at λ = 2091 nm. The blooming was carried out in order to reduce the possible effect of the interference field of the incident and reflected waves on the initialisation of optical damage, since the reflection coefficient from the uncoated ZGP surface is ~25%. On the working faces of samples 7–9, antireflection coatings (with a transmission of more than 98% at λ = 2091 nm) were applied on both sides.

The parameters of the experimental samples and the technological operations carried out with them are shown in Table 2.

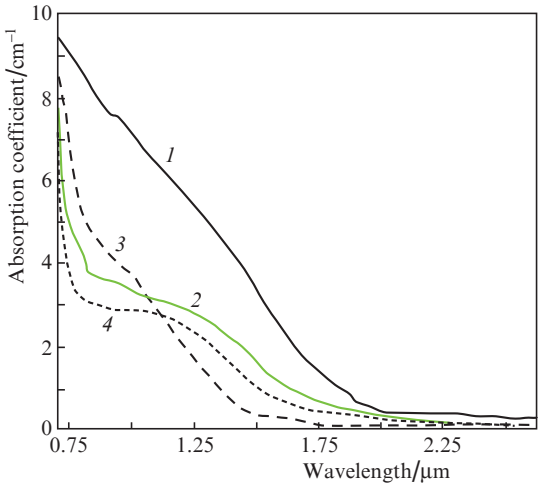

Figure 2. Absorption spectra in the wavelength range 0.75–2.6 μm for ZGP plates cut from crystal I immediately after growth (*1*), after annealing at 600 °C (*2*) and after irradiation with a fast electron flow (*3*), as well as for the plate ZGP cut from crystal II after annealing at 600 °C (*4*).

Using a SHIMADZU UV-3600 spectrometer, absorption spectra were obtained in the wavelength range 0.7–2.5 μm for ZGP plates 1 mm thick, additionally cut from single crystals I and II (Fig. 2). The absorption coefficient in plates from crystal II after annealing turned out to be ~0.25 cm^{-1} less than the absorption coefficient in plates from crystal I after annealing in almost the entire measurement range.

The control of the profiles of the working surfaces of the samples under study was implemented by means of a ZYGO NewView 7300 profilometer using the white light interferometry method. The profilometer and its software allow measurements with $50^{\times}$ magnification (Fig. 3). For each experimental sample, surface areas with a size of 110 × 110 μm were investigated and the following parameters were estimated (their values are given in Table 2):

1) the maximum difference in the height and depth of inhomogeneities on the surface (PV) relative to the average value;

2) the root-mean-square roughness depth

$$\mathrm{RMS} = \sqrt{\frac{1}{l}\int_0^l z^2(x)\,\mathrm{d}x}\,, \qquad (1)$$

Table 2. Parameters of the studied ZGP samples.

Sample	Postgrowth treatment	Absorption coefficient at λ = 2091 nm/cm^{-1}	Type of polishing procedure	Polishing parameters		
				PV/nm	RMS/nm	R_a/nm
1	A	0.5	D, E	33.7	1.23	0.83
2	A	0.5	D	40.6	1.38	1.08
3	A	0.5	D, E, F	48.6	0.36	0.15
4	B	0.3	D, E, F	31.4	0.44	0.27
5	B	0.3	D, E, F	37.1	0.49	0.17
6	B, C	0.03	D, E, F	31.4	0.44	0.27
7	B, C	0.03	D, E, F	32.6	0.45	0.21
8	B, C	0.03	D, E, F	40.6	0.37	0.22
9	B, C	0.03	D, E, F	40.6	0.37	0.22

Note: PV PV is the maximum difference in height and depth of inhomogeneities on the surface relative to the average value; RMS is the root mean square roughness depth; and R_a is the arithmetic mean deviation of the roughness profile from the centre line.

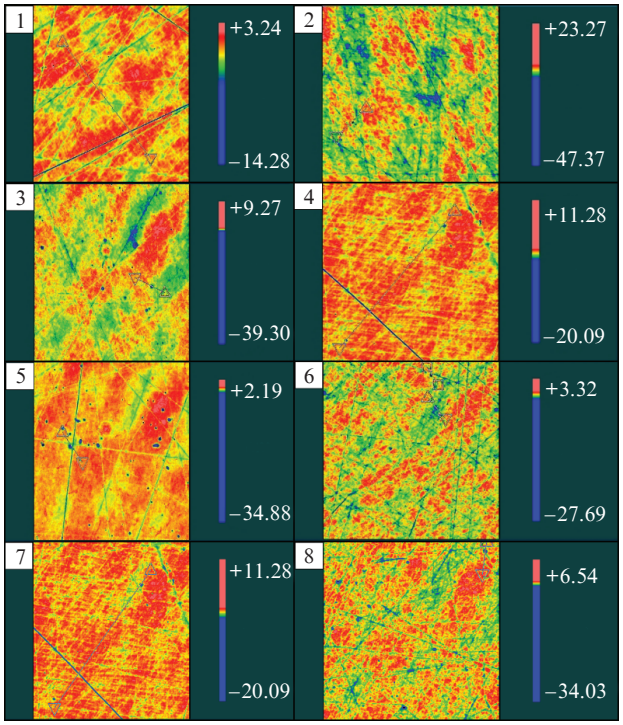

Figure 3. (Colour online) Surface profiles of the ZGP samples under study (in nanometres). The number of the image corresponds to the number of the sample under study (from 1 to 8); the profiles of the surfaces of samples 8 and 9 are the same.

where l is the base length in the direction of the x axis along which the roughness profile is estimated [26]; z is the axis normal to the surface; $z(x)$ is the distance from the centre line of the roughness profile to the surface roughness curve at a point with the x coordinate; and

3) the arithmetic mean deviation of the roughness profile from the midline [26]

$$R_a = \frac{1}{l}\int_0^l |z(x)|\,\mathrm{d}x. \qquad (2)$$

3. Experimental setup

As a radiation source with a wavelength of 2091 nm, we used a Ho^{3+}:YAG laser, developed and manufactured at the IAP RAS [27], pumped by a cw thulium fibre laser. The Ho^{3+}:YAG laser operated in the active Q-switched regime with a pulse width $\tau_p = 18-45$ ns, which changed depending on the pulse repetition rate f varied in the range 12–40 kHz (Fig. 4).

The amplitude of nanosecond pulses, their width and energy, as well as the beam diameter, were stable at constant pumping (random variations in the pulse amplitude did not exceed 5%) [27]. Upon increasing the pump, the amplitude of the lasing pulses changed in proportion to the increase in the average radiation power with an insignificant change in the pulse width and beam diameter. The total number of pulses was determined by their repetition rate and exposure time. For each separate series of measurements at the same pulse repetition rate, their number remained unchanged during the exposure. To avoid changing the pulse width and the shape of the generated Ho^{3+}:YAG laser beam, the average radiation

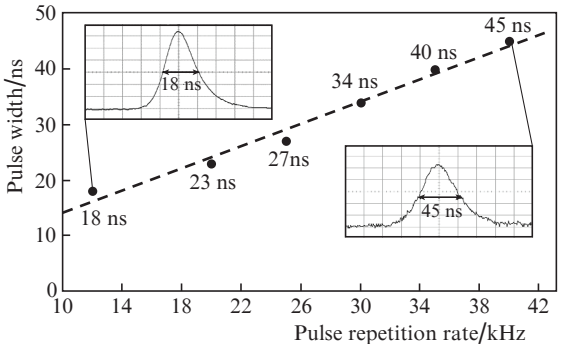

Figure 4. Dependences of the laser pulse width on their repetition rate for a Ho^{3+}:YAG laser.

power of the thulium fibre pump laser in all experiments was kept the same and equal to ~50 W. The maximum average radiation power generated by the Ho^{3+}:YAG laser was 30 W in a linearly polarised high-quality Gaussian beam (parameter $M^2 \leqslant 1.2$).

As a radiation source at a wavelength of 1064 nm, we used a Nd^{3+}:YAG laser from LLC 'LOC' ($f = 3$ kHz, $\tau_p = 50$ ns).

The average laser power P_{av} was measured before each experiment with power meters (Coherent PM10 with FieldMaxII indicator or Gentec UP25N-40S with a SOLO indicator) installed in the plane of the test sample.

The optical scheme of the experimental setup (Fig. 5) included a Ho^{3+}:YAG or Nd^{3+}:YAG laser (1), an optical Faraday isolator (FI), a half-wave plate $\lambda/2$, a polarising mirror (M1) with high transmission for p-polarisation and high reflection for s-polarisation at the working wavelength, a two-lens Galilean telescope (T), a sample under study, and a power meter (PM). The diameter of the laser beam in the testing plane corresponding to the input aperture of the plate under test was measured by the Foucault knife method [28]. The measured radiation beam diameter d in all experiments (except those described in Sections 6 and 7) was 270 ± 10 μm at the e^{-2} level of the maximum intensity (Rayleigh length of the focal waist z_R = 27.4 ± 2.2 mm). The power level was controlled using an attenuator consisting of a half-wave plate and a polarising mirror. To prevent the reflected radiation from entering the laser, the samples (plates) under study were deviated from the position corresponding to normal incidence by 3°, which, like the presence of a Faraday isolator in the circuit, prevented an uncontrolled change in the parameters of the incident radiation.

The processes occurring in the crystal in the predamage period and during the damage were visualised using a digital holographic camera (DHC) similarly to Ref. [17]. The DHC consisted of a laser diode with a wavelength of 1064 nm (ML150-638/1060-040-TTL-FK-m, 'Laser Engineering and Technology', Minsk), and objective lens (L) forming a plane-parallel beam, and a CCD camera (VCXU31M , Baumer, Switzerland). To register the damage process in samples with polished lateral surfaces (8 and 9), the DHC was located at position 1, and to register the process of optical damage in thin plates 1–7, the camera was at position 2.

The laser beam was monitored using a Pyrocam IV pyrocamera (Ophir-Spiricon) at a sampling rate of 100 fps (Fig. 6). During the exposure time (up to 30 s), the beam image remained stable. According to the international standard

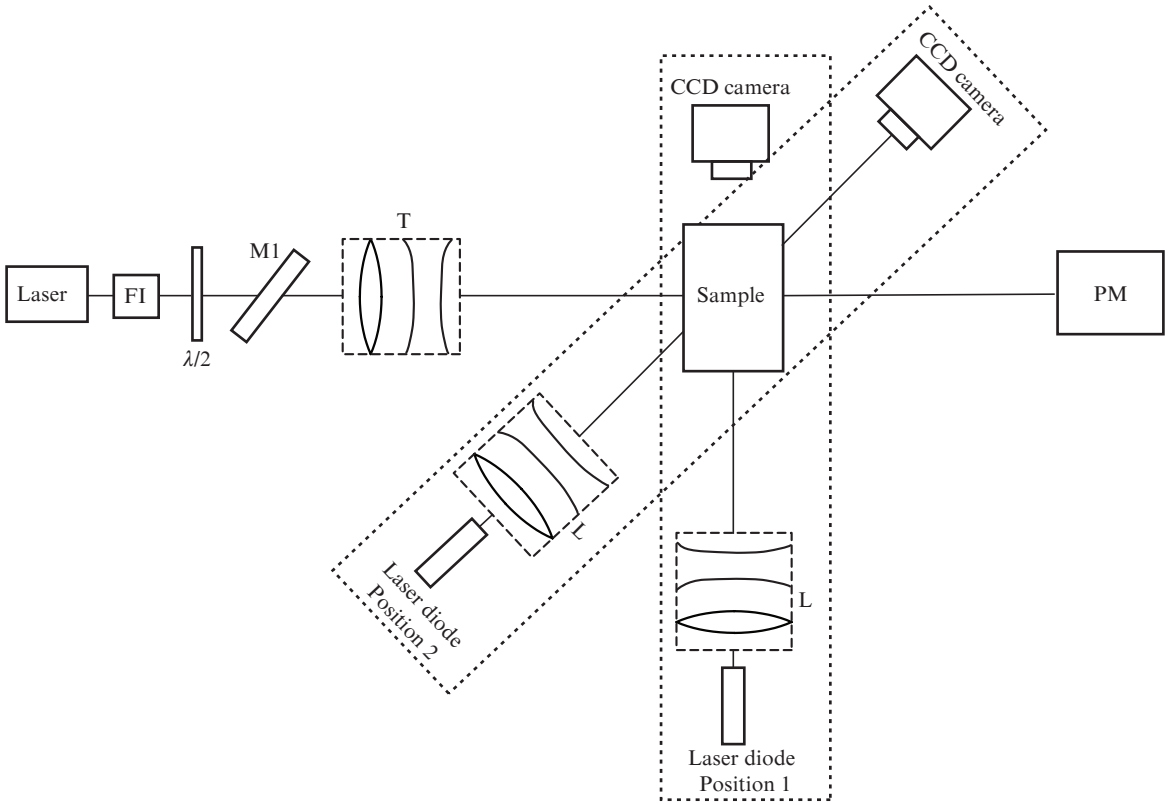

Figure 5. Optical layout of the experimental setup.

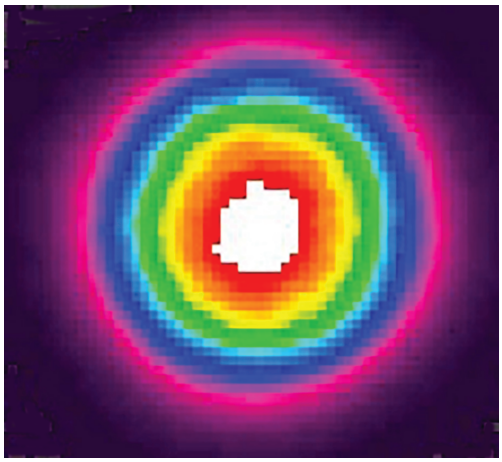

Figure 6. (Colour online) Intensity distribution of the laser beam behind the focus of the lens, obtained using a Pyrocam IV laser beam profile meter.

ISO11146, the effective area of a Gaussian beam was determined as $\pi d^2/8$ [28], and the energy density of laser radiation was

$$W = 8P_{av}/(f\pi d^2). \quad (3)$$

Studies of the LIDT using Ho^{3+}:YAG laser radiation were carried out in rooms corresponding to 6 ISO and 4 ISO ranges of purity (according to [29]). No differences were found in the ZGP LIDT in these premises.

4. Method for determining the laser-induced damage threshold of $ZnGeP_2$

To determine the LIDT of crystals, two standard methods, S-on-1 an R-on-1, are used. The S-on-1 technique described in the international standard ISO 11254-2 [30] allows taking into account the probabilistic nature of optical damage, but requires a large surface area of the test sample, which is not always possible in practice.

The essence of the R-on-1 technique is that each individual region of the crystal is irradiated with a laser beam with a gradual increase in power until an optical damage or a predetermined value of the energy density is reached. The method for determining the R-on-1 LIDT, which is more acceptable from the point of view of practical application, requires less space on the sample surface and therefore can be used for samples with a limited aperture [31]. It was earlier shown [16] that both methods give comparable results in relation to the determination of ZGP LIDT at wavelengths of ~2100 and 1064 nm at their repetition rates 1–10 kHz and pulse widths of 20 ns.

In our work, LIDT studies were carried out according to the R-on-1 technique with an exposure time τ_{ex} = 1 s and pulse repetition rates of 12, 20, 25, 30, and 35 kHz. First, the samples under study were exposed to laser pulse packets with a fixed energy density in each pulse of 0.1 J cm^{-2} (for Ho^{3+}:YAG laser radiation) and 0.01 J cm^{-2} (for Nd^{3+}:YAG laser radiation), which did not cause damage to the crystal surface. Then the energy density was increased with a step of ~0.2 J cm^{-2} for the Ho^{3+}:YAG laser and with a step of 0.001 J cm^{-2} for the Nd^{3+}:YAG laser. The fact of optical damage was established by the appearance of a glow in the

region of action and a decrease in the radiation transmittance. Then the plate was moved 0.8 mm in height or width using a three-coordinate slide; the experiment was repeated five times with subsequent statistical data processing. The interval between the series of irradiation in all experiments on testing the LIDT was fixed and amounted to ~2 min. This time interval seems to be sufficient for relaxation of reversible changes in parameters in the region of the crystal exposed to laser radiation. In particular, during this time a relaxation of the temperature and concentration of free charge carriers to the initial state occurs.

The optical damage probability was obtained by plotting the cumulative probability at different optical damage energy densities. The LIDT value (W_{0d}) was taken to be the energy density corresponding to the approximation of the optical damage probability to zero, $P_d = 0$.

For each series of measurements, after which an optical damage was observed, the average value of the threshold energy density W_{av} and the rms error of its determination $\langle \Delta W_{av}^2 \rangle$ were calculated according to the formulae:

$$W_{av} = \frac{\sum W_i n_i}{N}, \tag{4}$$

$$\langle \Delta W_{av}^2 \rangle = \frac{\sum (\langle W_{av} \rangle - W_i)^2 n_i}{N(N-1)}, \tag{5}$$

where N is the total number of damaged areas; W_i is the threshold energy density in one of the irradiated regions; and n_i is the number of regions with the damage threshold W_i.

To find the LIDT confidence interval

$$W_d = W_{av} \pm k \langle \Delta W_{av}^2 \rangle^{1/2}, \tag{6}$$

where k is the Student's coefficient, the Student's t-distribution was used for the confidence probability [32, 33]

$$F(k,N) = \frac{\Gamma(N/2)}{\sqrt{\pi(N-1)}\,\Gamma(N-1)/2} \int_{-k}^{k} \left(1 + \frac{z^2}{V-1}\right)^{-N/2} \mathrm{d}z, \tag{7}$$

where Γ is the gamma function.

Tables 3–5 show the results of statistical processing of the experimentally measured data using the parameters determined by expressions (4)–(7).

Figures 6–9 and 13 show the results of LIDT measurements using the R-on-1 method.

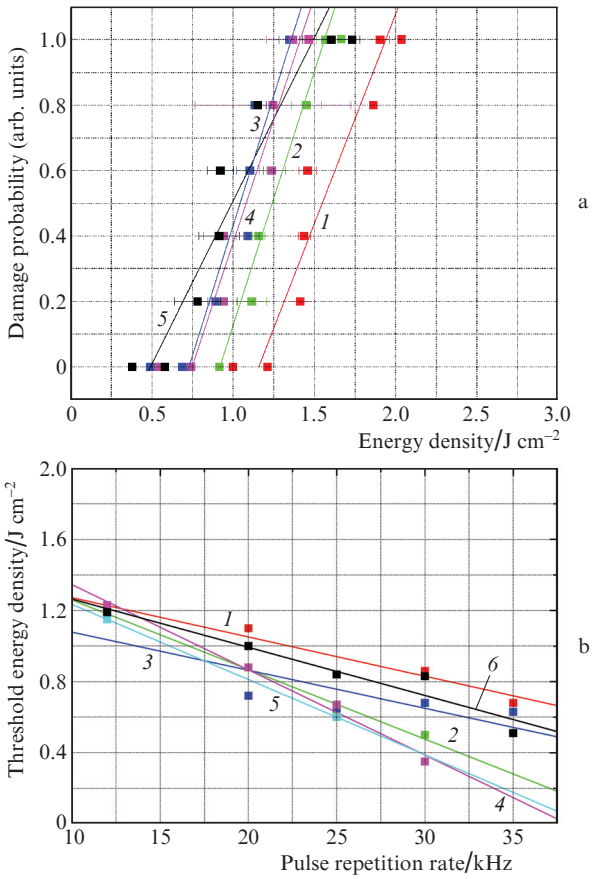

Figure 7. (Colour online) Probability of optical damage of sample 6 s. the energy density of laser radiation at an exposure time τ_{ex} = 1 s for f = (*1*) 12, (*2*) 20, (*3*) 25, (*4*) 30, and (*5*) 35 kHz (a); threshold energy density W_{0d} vs. f for samples 1–6 (lines *1*–*6*, respectively) (b).

5. Influence of postgrowth treatments and crystal defects on LIDT

The LIDT values of samples with different technological history were determined (see Tables 3 and 5). As an example of the results obtained, Fig. 7a shows the dependences of the optical damage probability on the energy density of the testing laser radiation for sample 6, and Fig. 7b shows the dependences of the threshold energy density W_{0d} on the pulse repetition rate for samples 1–6.

Table 3. Damage threshold parameters at a wavelength of 2091 nm at f = 12 kHz and τ_{ex} = 1 s, as well as sample polishing parameters.

Sample	N	$\langle \Delta W_{av}^2 \rangle^{1/2}$/J cm^{-2}	k	W_{av}/J cm^{-2}	W_d/J cm^{-2}	W_{0d}/J cm^{-2}	Polishing parameters		
							PV/nm	RMS/nm	R_a/nm
1	5	0.01	2.8	1.6	1.6 ± 0.3	1.2 ± 0.1	33.7	1.23	0.83
2	5	0.02	2.8	2.0	2.0 ± 0.1	1.2 ± 0.1	40.6	1.38	1.08
3	4	0.2	3.2	1.9	1.9 ± 0.4	1.2 ± 0.1	48.6	0.36	0.15
4	5	0.2	2.8	1.9	1.9 ± 0.5	1.2 ± 0.1	31.4	0.44	0.27
5	4	0.09	3.2	1.6	1.6 ± 0.3	1.2 ± 0.1	37.1	0.49	0.17
6	5	0.08	2.8	1.6	1.6 ± 0.2	1.2 ± 0.1	31.4	0.44	0.27

Note: N is the number of measurements; $\langle \Delta W_{av}^2 \rangle^{1/2}$ is the standard deviation; k is the Student's coefficient at a confidence level of 0.95; and W_{av} is the average value of the energy density taking into account the measurement error W_d and the energy density W_{0d} at a zero probability of optical damage.

The calculated damage parameters for samples 1–6 are given in Table 3; for convenience of comparison, the parameters of the polishing of the samples are also presented.

Based on the results presented in Tables 2, 3 and in Figs 2 and 7, it can be concluded that low-temperature annealing (at a temperature of ~600 °C) leads to a decrease in linear absorption in the entire transparency region of crystals [see Fig. 2, curves (*2*) and (*4*)], which is also confirmed by the results of [34]. Irradiation with fast electrons of single crystal I also causes a decrease in linear absorption in the spectral region $\lambda > \mu$m (due to a change in the energy spectrum of deep levels of initial point defects [34]), but leads to an increase in absorption in the wavelength region $\lambda < 1.2$ μm. When analysing the data presented in Fig. 7 and in Table 3, it can be seen that, despite the indicated changes in the absorption spectrum of samples cut from single crystal I, the LIDT in ZGP at $\lambda = 2091$ nm remains independent of the performed postgrowth operations.

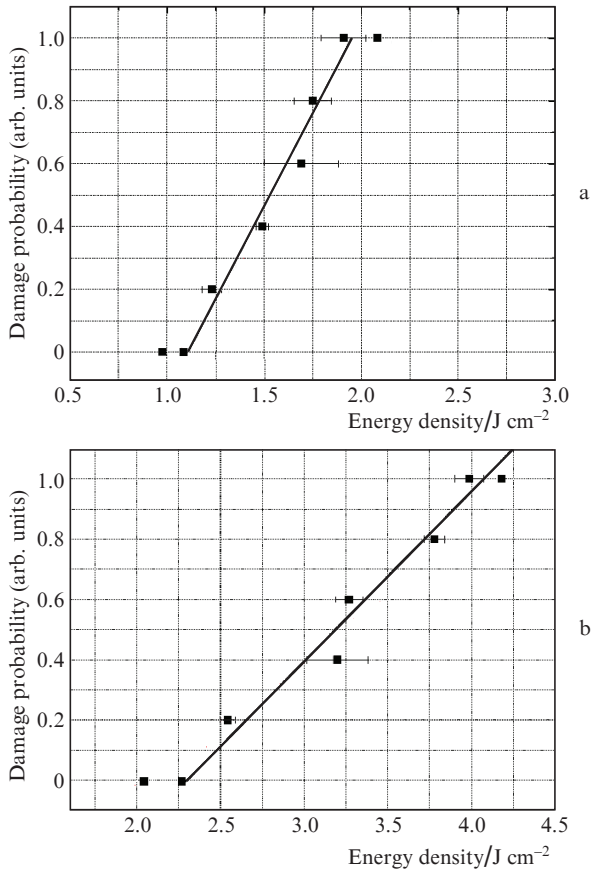

Figure 8. Damage probabilities of sample 7 cut from single crystal I (a) and sample 8 cut from single crystal II (b) measured by the R-on-1 method.

Table 4. Comparison of the LIDT of single crystals I (sample 7) and II (sample 8) for $\tau_{ex} = 1$ s и $f = 12$ kHz at $\lambda = 2091$ nm.

Sample	N	$\langle \Delta W^2_{av} \rangle^{1/2}$/ J cm^{-2}	k	W_{av}/ J cm^{-2}	W_d/ J cm^{-2}	W_{0d}/ J cm^{-2}
7	5	0.042	2.8	1.6	1.6 ± 0.1	1.2 ± 0.1
8	5	0.24	2.8	3.4	3.4 ± 0.7	2.26 ± 0.08

Note: The parameters are the same as in Table 3.

Using ZGP samples 7 and 8, the LIDT of single crystals I and II was compared at $\tau_{ex} = 1$ s and $f = 12$ kHz at $\lambda = 2091$ nm (Fig. 8 and Table 4).

Comparison of the results presented in Figs 2 and 8, as well as in Tables 3 and 4, shows that the LIDT of single crystal ZGP II with lower absorption at wavelengths 0.7–2.5 μm is more than twice the LIDT of single crystal I with higher absorption in this spectral range. Since these single crystals have the same impurity composition and no bulk defects and foreign phases were found in them, the data obtained could be explained by the difference in the concentration of crystal lattice dislocations in single crystals I and II. It can be assumed that lattice dislocations, which manifest themselves in an increase in scattering losses during propagation of radiation through the crystal, affect the LIDT. This influence can be associated with a decrease in the surface strength of elements in the presence of dislocations, as well as with the appearance of additional impurity levels in the band gap, which affect absorption. Thus, an increase in the concentration of lattice dislocations decreases the LIDT. Based on the results of measuring the spectral dependence of the transmission of the samples [Fig. 2, curves (*2*) and (*4*)], it can be asserted that the concentration of dislocations in single crystal II is much lower than in single crystal I. Exposing crystals to a flux of fast electrons and annealing allows changing the concentration of point defects and the position of their energy levels in the band gap of the crystal, but cannot change the concentration of dislocations, which is determined by the synthesis parameters of the ternary compound and the growth of the ZGP single crystal. Thus, the assumption about the dominant effect of dislocations on the LIDT in the spectral region of ~2 μm allows us to explain the experimental data obtained, namely, the independence of the damage threshold from postgrowth treatments, but a strong correlation of this threshold with the optical transmission of the initial ZGP samples that were not subjected to postgrowth treatments.

As is known, the quality of surface polishing significantly affects the radiation resistance of the material; therefore, RMS and PV are considered the most informative parameters of the effect of polishing on the LIDT [15]. For ZGP crystals, it was shown [15] that when the RMS parameter changes by a factor of two, and the PV parameter by more than five times, the LIDT in energy density changes in the same way, by two times. At the same time, the results presented in Table 3 show that with an almost unchanged polishing parameter PV, but with the RMS parameter varied by more than four times and the R_a parameter by more than five times, the LIDT did not change. Based on this, we can conclude that PV is the most informative parameter characterising the influence of the polishing quality of the ZGP working surface on the LIDT. It can be assumed that it is the irregularities of the polished surface (peaks and valleys) described by the PV parameter that contribute to the optical damage mechanism and can be seed inhomogeneities for the initiation of optical damage due to field effects at a wavelength of 2091 nm.

6. Influence of exposure time, laser beam diameter, and crystal temperature on the laser-induced damage threshold

The influence of the exposure time and laser beam diameter on the LIDT of a ZGP crystal at room temperature was studied, as well as the effect of the crystal temperature on the

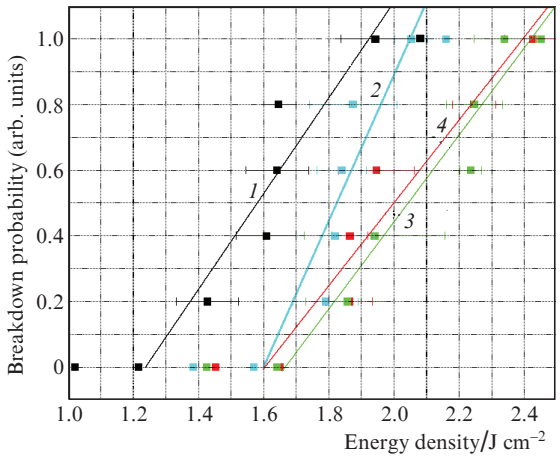

Figure 9. (Colour online) Probability of optical damage vs. the energy density of laser radiation at $\lambda = 2091$ nm, $\tau_{ex} = (1)$ 30, (2) 10, (3) 5 and (4) 2 s.

LIDT when exposed to Ho^{3+}:YAG laser radiation (at λ = 2091 nm). The measurements were carried out according to the R-on-1 technique at $f = 12$ kHz and $\tau_p = 18$ ns. The effect of the laser beam diameter and crystal temperature on the LIDT was measured at $\tau_{ex} = 1$ s.

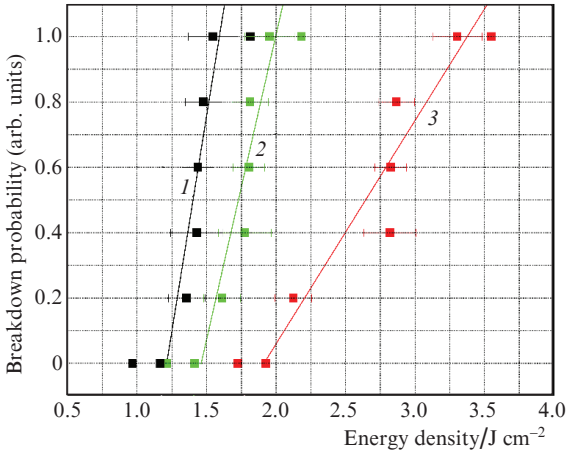

Figure 10. Optical damage probability vs. the energy density of laser radiation at $\lambda = 2091$ nm at $\tau_{ex} = 1$ s and beam diameters of (1) 580, (2) 300, and (3) 200 μm.

To study the effect of exposure time and laser beam diameter on the LIDT, sample 9 was used, which was similar to sample 8 in optical parameters and processing. It was shown that with an increase in the exposure time from 2 to 30 s, the LIDT decreases by a factor of 1.2, from 1.57 to 1.28 J cm^{-2} (Fig. 9).

Measurements at room temperature showed that with a decrease in the laser beam diameter by a factor of 2.9, the LIDT increased from 580 to 200 μm (at the e^{-2} level), and W_{0d} increased by a factor of 1.4, from 1.32 to 1.91 J cm^{-2} (Fig. 10)

An increase in the LIDT with a decrease in the laser beam diameter and a decrease in the LIDT with an increase in the exposure time can be explained by the influence of accumulating thermal effects when the crystal is exposed to radiation with a wavelength of 2091 nm.

To study the temperature dependence of the LIDT, samples 8 and 9 were placed in a sealed cuvette filled with dry nitrogen at normal pressure. Using a calorimeter beaker filled with liquid nitrogen and having a thermal contact with the cuvette, the samples were cooled to –106 °C (the sample temperature was monitored with an electronic thermometer). The cuvette windows were made of crystalline sapphire without antireflection coatings with a transmittance (at $\lambda = 2091$ nm) of ~85%. The incident laser beam was focused on the front face of sample 8 into a spot with a diameter of $d \approx 100$ μm, and on the front face of sample 9 into a spot with a diameter of $d \approx 270$ μm.

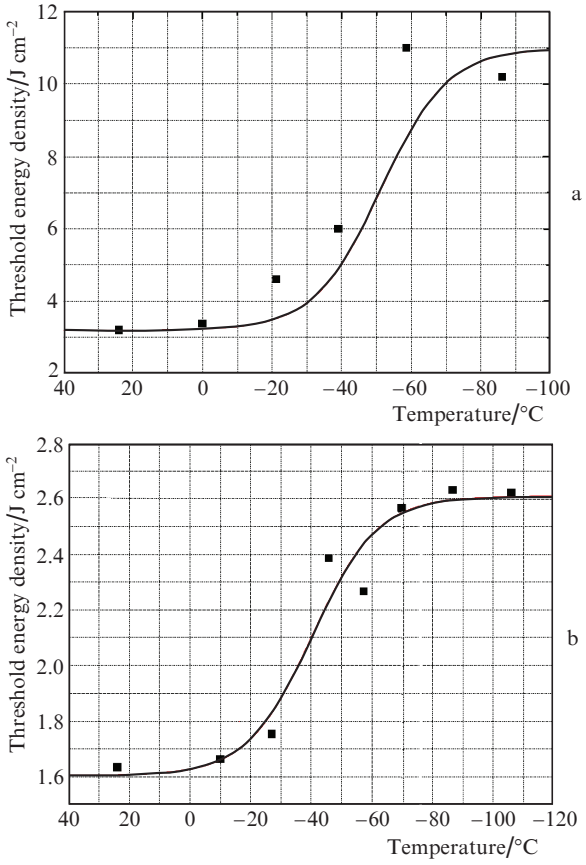

Figure 11. Optical damage energy density W_{0d} vs. the temperature of the ZGP crystal exposed to Ho^{3+}:YAG laser radiation at $\lambda = 2091$ nm, the laser beam diameter being (a) 100 and (b) 270 μm.

At room temperature and a laser beam diameter of 270 μm, the threshold values of damage for sample 8 were: $W_{0d} = 2.3$ J cm^{-2} and $W_d = 3.4 \pm 0.4$ J cm^{-2}. The measurement results demonstrated a significant increase in the LIDT (W_{0d} values), which is especially noticeable when the temperature decreases from +20 to –60 °C (Fig. 11a). At temperatures from +24 to –86 °C and a laser beam diameter of 100 μm, W_{0d} increased more than threefold (from 3.2 to 10.2 J cm^{-2}); however, at temperatures below –60 °C, the increase in the LIDT stopped.

Measurements of the dependence of the LIDT on the crystal temperature were also carried out for sample 9 with a laser beam diameter of 270 μm (Fig. 11b). At positive temperatures, the change in the LIDT was weak, at temperatures from zero to –60 °C, an increase in W_{0d} by more than 1.5

times was observed (from 1.6 to 2.6 J cm^{-2}), at temperatures below –60 °C, the increase in the LIDT also stopped.

It is known that ZGP is a high-resistance semiconductor with stable hole conductivity, the value of which is difficult to change [35]. A typical temperature dependence of the concentration of free charge carriers in ZGP is described by an exponential curve with an activation energy of deep impurity centres of 0.3–0.6 eV [36]. However, the obtained temperature dependence of the LIDT has a sigmoidal character and therefore cannot be explained by absorption on free carriers (holes) arising from the ionisation of individual point defects.

The obtained temperature dependence of the LIDT can be explained by the temperature dependence of the occupation numbers of phonons, which, together with optical quanta, participate in indirect transitions of nonlinear absorption from the valence band to the impurity level [37]. In support of this assumption, it can be noted that, with decreasing temperature, the occupation numbers of phonons in the crystal lattice increase, leading to a decrease in the probability of their participation in indirect transitions of electrons from the valence band to impurity levels.

7. Registration of processes in the predamage period by digital holography

The processes occurring in the crystal in the predamage region of parameters and during the damage were visualised by DHC using the scheme presented in Fig. 4 (with the power action of radiation at a wavelength of 2091 nm and visualisation by a beam of laser radiation at a wavelength of 1064 nm).

In most experiments (~85% of the total number of measurements), optical damage began at the exit surface of the sample, forming a breakdown track ending at the entrance surface. Under the action of laser pulses, a luminous spherical region with a transverse size of 0.7–1 mm appeared on the output surface of the ZGP crystal, which then moved in the crystal inside the laser beam channel towards the input surface, forming a breakdown track. Visualisation of the optical damage process was carried out using DHC according to the previously described method [17]. The formation of an optical damage track in ZGP crystals and the mechanism of its formation are presented in more detail in [17].

Since both working surfaces of the tested samples were located behind the focal plane, and their thickness was less (or much less in the case of plates 1–7) than the length of the focal waist of the beams z_R, the predominant onset of damage on the output surface can be explained by the influence of predamage nonlinear effects. Direct measurements of the spatial structure of the beam (at a wavelength of 2091 nm) after passing through the samples at low power did not reveal its significant distortions in comparison with the initial Gaussian profile in any of the elements used. In this regard, the predominant development of damage from the output surface of the samples can be associated with the influence of nonlinear self-focusing, which under experimental conditions can be caused by thermal, striction, or electronic nonlinearity of ZGP [12, 15, 38]. Numerical calculations of the thermal lens, carried out earlier for ZGP samples under similar exposure conditions, showed its noticeable effect on the beam structure [39, 40].

Comparative studies of the crystal before, during, and after the damage established the fact that the radiation propagation channel in sample 8 darkened at a laser energy density of more than 1.8 J cm^{-2} at a wavelength of 2091 nm. Visually, this effect manifested itself in the reconstructed images of the plane of the best setting in the form of a darkening of the crystal region in which this radiation propagated (Fig. 12). This process is clearly demonstrated in Fig. 12b: a dark track is formed in the propagation channel of a beam of intense laser radiation at a wavelength of 2091 nm (with testing radiation at λ = 1064 nm). The darkening is reversible: with a decrease in the energy density of the incident radiation to 1.8 J cm^{-2} or less, or upon the complete cessation of laser action on the crystal, the darkening region disappears (Fig. 12c). The relaxation time of the darkening region of the laser channel was found to be less than 5 ms; further refinement of this time was limited by the response speed of the CCD matrix.

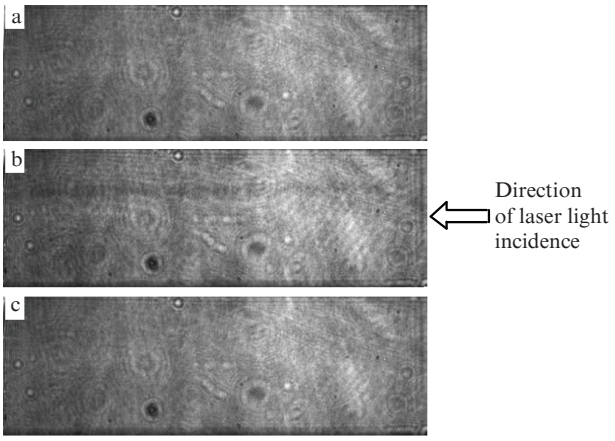

Figure 12. Reconstructed image of the volume hologram of a ZGP single crystal (sample 8) before the test (a), when exposed to pulsed radiation of a Ho^{3+}:YAG laser with an energy density of 1.8 J cm^{-2} (b), and 10 ms after termination of radiation exposure (c).

The darkening of the channel of propagation of high-power laser radiation in the predamage region can be explained by a local decrease in the ZGP band gap upon heating. Indeed, it is known that the band gap of semiconductors decreases with increasing temperature [41]. This leads to an increase in the absorption of the test beam at λ = 1064 nm.

8. Threshold of optical damage of ZGP at a wavelength of 1064 nm

LIDT studies of samples 3 and 6 were carried out by the R-on-1 method using Nd^{3+}:YAG laser radiation at a wavelength of 1064 nm. In all the experiments performed, the damage began on the front surface of the sample. The difference between the samples under study was that plate 6 was exposed to a flow of fast electrons and had an absorption of ~4 cm^{-1} at a wavelength of 1064 nm, while plate 3 was not exposed

Table 5. Damage threshold at λ = 1064 nm with f = 3 kHz.

Sample	N	$\langle \Delta W_{av}^2 \rangle^{1/2}$/ J cm^{-2}	k	W_{av}/ J cm^{-2}	W_d/ J cm^{-2}	W_{0d}/ J cm^{-2}
3	5	0.01	2.8	0.31	0.31 ± 0.01	0.02 ± 0.05
6	5	0.02	2.8	0.72	0.72 ± 0.03	0.17 ± 0.005

Note: The parameters are the same as in Table 3.

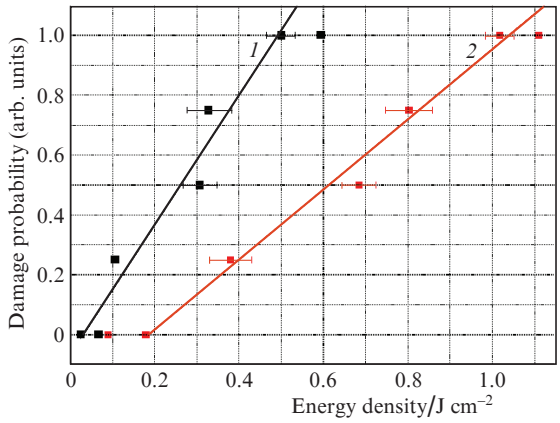

Figure 13. Probability of optical damage vs. the energy density of laser radiation at $\lambda = 1064$ nm, $\tau_{ex} = 1$ s, and $f = 3$ kHz for samples 3 (*1*) and 6 (*2*).

and its absorption was ~7.5 cm^{-1}. As can be seen from Fig. 13 and Table 5, upon exposure of the ZGP plate to a flow of fast electrons, the LIDT increased threefold with a twofold decrease in the linear absorption. This indicates that when exposed to radiation at $\lambda = 1064$ nm, the optical damage of ZGP occurs due to single-photon absorption, which can be explained by the presence of point defects in the single crystal. This conclusion is in good agreement with the previously obtained results [16].

9. Conclusions

The studies have revealed a number of parameters of ZGP single crystals, their postgrowth processing, as well as exposure to radiation, which have the strongest effect on the LIDT. It was shown that ZGP single crystal II, whose absorption in the wavelength range 0.7–2.5 μm after annealing is less than the absorption of single crystal I by ~0.25 cm^{-1}, has almost twice the LIDT at a wavelength of 2091 nm (2.26 J cm^{-2} at $f = 12$ kHz and $\tau_{ex} = 1$ s) than single crystal I (1.2 J cm^{-2} at the same parameters) with higher absorption in this range. The difference in the transmission spectra of these samples in the wavelength range 0.7–2.5 μm became an indicator of the difference in the LIDT of the samples. At the same time, it was found that thermal annealing of ZGP and its irradiation with a flow of fast electrons do not lead to an increase in the LIDT at a wavelength of 2091 nm, although they can reduce the absorption by an order of magnitude in a wide spectral range ($\lambda \approx 1.2$–2.5 μm) due to a change in the energy spectrum of deep levels of initial point defects. The obtained results on the LIDT can be explained by the difference in the concentration of dislocations of the crystal lattice of ZGP elements, which affect the surface strength of the elements and optical absorption (due to the appearance of impurity levels in the band gap). The difference in the concentration of dislocations in the samples is manifested in their transmission spectrum, primarily because of scattering of radiation by mechanically stressed regions around the dislocations. Thermal annealing at the indicated temperatures and exposure to a flow of fast electrons do not affect the concentration of dislocations in the crystal lattice and, therefore, the LIDT at a wavelength of 2091 nm.

It is shown that the influence of the quality of polishing of the ZGP surface on the LIDT is determined to the greatest extent by the PV parameter. The irregularities of the polished surface (peaks and valleys) characterised by this parameter are, apparently, seed inhomogeneities for the initiation of optical damage due to field effects.

It was revealed that the LIDT increased by a factor of 1.4 (from 1.32 to 1.91 J cm^{-2}) with a decrease in the laser beam diameter by 2.9 times (from 580 to 200 μm) and an increase in the LIDT by a factor of 1.2 (from 1.28 to 1.57 J cm^{-2}) with a decrease in the exposure time from 30 to 2 s, as well as an increase in the LIDT with a decrease in the repetition rate of nanosecond radiation pulses at $\lambda = 2091$ nm.

A strong dependence of the LIDT at $\lambda = 2091$ nm and $f = 12$ kHz on the crystal temperature varying from +24 to –106 °C was found. As the temperature decreases from zero to –60 °C, a sharp increase in the threshold energy density is observed: from 1.6 to 2.6 J cm^{-2} at a laser beam diameter of 270 μm and from 3.2 to 10.2 J cm^{-2} at a diameter of 100 μm (by 1.5 and 3 times, respectively). The increase in the LIDT with decreasing ZGP temperature can be explained by the temperature dependence of the occupation numbers of phonons, which, together with optical quanta, participate in indirect transitions from the valence band to the impurity level. An increase in the occupation number of phonons with a decrease in the crystal temperature leads to a decrease in the probability of their participation in indirect transitions of electrons from the valence band to impurity levels and, consequently, to a decrease in the nonlinear absorption of the crystal in the predamage region of parameters.

Reversible photodarkening of the propagation channel of high-power laser radiation at $\lambda = 2091$ nm in the ZGP in the predamage region of parameters has been established. This photodarkening can be explained by a local decrease in the band gap of ZGP upon heating. It is shown that, when the ZGP is exposed to radiation at $\lambda = 1064$ nm, the linear single-photon absorption of the material, which can be explained by the presence of point defects in the crystals under study, makes a significant contribution to the optical damage mechanism and determines the value of its threshold.

The results presented show the main dependences of the LIDT in Russian-made ZGP crystals with a certain concentration of impurities, dislocations, and point defects, as well as postgrowth processing, on the experimental conditions. The maximum LIDT measured at room temperature in our study was 3.2 J cm^{-2} at $\lambda = 2091$ nm at a pulse repetition rate of 12 kHz, a pulse width of 18 ns, and a beam diameter of 100 μm on the surface of the test sample. With comparable parameters of the testing laser radiation (wavelength 2050 nm, pulse repetition rate 10 kHz, pulse width 15 ns, beam diameter on the surface of the tested sample 130 μm) in measurements by other authors of the LIDT of ZGP crystals (manufactured by BAE Systems, USA) in 2006 was ~2 J cm^{-2} [15]. In the paper of 2018 [42], a significant increase in the LIDT, up to more than 4 J cm^{-2} at a wavelength of 2091 nm at a pulse repetition rate of 10 kHz and a pulse width of 20 ns, was indicated in improved ZGP crystals (also produced by Bae Systems). The existence of the world's best ZGP samples with a LIDT exceeding 4 J cm^{-2} [42] can be considered as confirmation of the possibility of achieving a better quality of nonlinear optical elements by improving their crystal structure and postgrowth processing conditions.

Acknowledgements. The research was supported by the Russian Foundation for Basic Research (Project No. 9-32-50094\19), as

well as Competitiveness Enhancement Programme of the Tomsk State University (Scientific Foundation of the TSU named after Dmitry I. Mendeleev). Experimental studies on determining the laser-induced damage threshold of ZGP under exposure to Ho^{3+}:YAG laser radiation were carried out with financial support from the Ministry of Science and Higher Education of the Russian Federation (State Assignment for the Institute of Applied Physics, RAS, Project No. 0035-2019-0012) and the Russian Science Foundation (Grant No. 19-12-00085).

References

1. Yevtushenko A., Rozniakowska-Klosinska M., in *Encyclopedia of Thermal Stresses* (Berlin: Springer, 2014) p. 2707–2719.
2. Parfenov V.A. *Lazernaya mikroobrabotka materialov* (Laser Microprocessing of Materials) (Saint-Petersburg: SPbGETU 'LETI', 2011) p. 59.
3. Bobrovnikov S.M., Matvienko G.G., Romanovsky O.A., Serikov I.B., Sukhanov A.Ya. *Lidarnyi spektroskopicheskii gazoanaliz atmosfery* (Lidar Spectroscopic Gas Analysis of the Atmosphere) (Tomsk: Institute of Atmospheric Optics, SB RAS, 2014).
4. Romanovskii O.A., Sadovnikov S.A., Kharchenko O.V., Yakovlev S.V. *Opt. Laser Technol.*, **116**, 43 (2019).
5. Kozub J., Ivanov B., Jayasinghe A., Prasad R., Shen J., Klosner M., Heller D., Mendenhall M., et al. *Biomed. Opt. Express*, **2**, 1275 (2011).
6. Schunemann P.G., Zawilski K.T., Pomeranz L.A., Creeden D.J., Budni P.A. *J. Opt. Soc. Am. B*, **33**, D36 (2016).
7. Hemming A., Richards J., Davidson A.A., Carmody N., Bennetts S., Simakov N., Haub J. *Opt. Express*, **21**, 1364 (2013).
8. Haakestad M.W., Fonnum H., Lippert E. *Opt. Express*, **22**, 8556 (2014).
9. Qian C., Yao B., Zhao B., Liu G., et al. *Opt. Lett.*, **44**, 715 (2019).
10. Bochkovsky D.A., Vasilyeva A.V., Matvienko G.G., Polunin Yu.P., et al. *Atmos. Ocean. Opt.*, **25**, 166 (2012) [*Opt. Atmos. Okeana*, **24**, 985 (2011)].
11. Soldatov A.N., Vasilyeva A.V., Polunin Yu.P., Kuksgauzen D.A., Kostyrya I.D. *Biotekhnosfera*, **3-4**, 47 (2012).
12. Manenkov A.A., Prokhorov A.M. *Sov. Usp. Phys.*, **29**, 104 (1986) [*Usp. Fiz. Nauk*, **148**, 179 (1986)].
13. Boling N.L., Crisp M.D., Dubé G. *Appl. Opt.*, **12**, 650 (1973).
14. Peterson R.D., Schepler K.L., Brown J.L. *J. Opt. Soc. Am. B*, **12**, 2142 (1995).
15. Zawilski K.T., Setzler S.D., Schunemann P.G., Pollak T.M. *J. Opt. Soc. Am. B*, **23**, 2310 (2006).
16. Hildenbrand A., Kieleck C., Tyazhev A., Marchev G., Stöppler G., Eichhorn M., Schunemann P.G., Panyutin V.L., Petrov V. *Opt. Eng.*, **53**, 122511 (2014).
17. Gribenyukov A.I., Dyomin V.V., Olshukov A.S., Podzyvalov S.N., Polovtsev I.G., Yudin N.N. *Russian Physics Journal*, **61** (11), 2042 (2019) [*Izv. Vyssh. Uchebn. Zaved., Ser. Fiz.*, **61**, 89 (2019)].
18. Andreev Yu.M., Badikov V.V., Voevodin V.G., Geiko L.G., Geiko P.P., Ivaschenko M.V., Karapuzikov A.I., Sherstov I.V. *Quantum Electron.*, **31**, 1075 (2001) [*Kvantovaya Elektron.*, **31**, 1075 (2001)].
19. Churnside J.H., Wilson J.J., Andreev Yu.M., Gribenyukov A.I., Shubin S.F., Dolgii S.I., Zuev V.V., in *NOAA Techn. Memorand. ERL WPL-224* (VA, USA, Springfield, 1992) p. 18.
20. Verozubova G.A., Filippov M.M., Gribenyukov A.I., Trofimov A.Yu., Okunev A.O., Stashchenko V.A. *Izv. Tomsk. Politekhnich. Univer.*, **321**, 121 (2012).
21. Brudny V.N., Voevodin V.G., Grinyaev S.N. *Phys. Solid State*, **48** (11), 2069 (2006) [*Fiz. Tverd. Tela*, **48**, 1949 (2006)].
22. Verozubova G.A., Gribenyukov A.I., Mironov Yu.P. *Inorg. Mater.*, **43**, 1040 (2007).
23. Dyomin V.V., Gribenyukov A.I., Podzyvalov S.N., Yudin N.N., Zinoviev M.M., Polovtsev I.G., Davydova A.S., Olshukov A.S. *Appl. Sci.*, **10**, 442 (2020).
24. Dyomin V.V., Gribenyukov A.I., Davydova A.S., Zinoviev M.M., Olshukov A.S., Podzyvalov S.N., et al. *Appl. Opt.*, **58**, G300 (2019).
25. Gribenyukov A.I., Yudin N.N., Podzyvalov S.N., Zinoviev M.M., Olshukov A.S., Shumeiko A.S., Soldatov A.N., Yudin N.A. *Opt. Mem. Neural Networks*, **29**, 147 (2020).
26. ISO 4287/1, *Surface texture: profile method – terms, definitions and surface texture parameters* (DC, USA, Washington: ANSI, 1997).
27. Antipov O.L., Kositsyn R.I., Eranov I.D. *Laser Phys. Lett.*, **14**, 015002 (2017).
28. ISO 11146-1:2005, *Lasers and laser-related equipment–Test methods for laser beam widths, divergence angles and beam propagation ratios* (DC, USA, Washington: ANSI, 2005).
29. ISO 14644-1-99, *Cleanrooms and associated controlled environments* (DC, USA, Washington: ANSI, 1999).
30. ISO 11254-2:2001, *Lasers and laser-related equipment – Determination of laser-induced damage threshold of optical surfaces – Part 1:1-on-1 test and Part 2: S-on-1 test* (DC, USA, Washington: ANSI, 2001).
31. http://lidaris.com/laserdamage-testing/.
32. ISO 2602:1980, *Statistical interpretation of test results – Estimation of the mean – Confidence interval* (DC, USA,Washington: ANSI, 1980).
33. Fisher R.A., Rothamsted M.A. *Metron.*, **5**, 90 (1925).
34. Gribenykov A.I., Verozubova G.A., Trofimov A., Yunda N.T., Vere A.W., Flyun C.J., in *Proc. 6 Intern. Conf. Modificat. Mater. Particle Beams and Plasma Flows* (Tomsk, 2002) p. 315.
35. Abrikosov N.Kh., Zemskov V.S. *Legirovannye poluprovodniki* (Doped Semiconductors) (Moscow: Nauka, 1975) p. 8.
36. Voevodin V.G. Doct. Thesis (Tomsk, SFTI, 2003).
37. Kopylov A.A., Pikhtin A.N. *Fiz. Tekh. Poluprovodn.*, **8**, 2398 (1974).
38. Shen I.R. *The Principles of Nonlinear Optics* (New York: Wiley, 2002; Moscow: Nauka, 1989).
39. Hutcheon R.J., Perrett B.J., Mason P.D. *Proc. SPIE 5620, Solid State Laser Technologies and Femtosecond Phenomena* (23 December 2004); https://doi.org/10.1117/12.577520.
40. Antipov O.L., Eranov I.D., Kositsyn R.I. *Quantum Electron.*, **47**, 601 (2017) [*Kvantovaya Elektron.*, **47**, 601 (2017)].
41. Pavlov P.V. *Fizika tverdogo tela* (Solid State Physics) (Moscow: Vysshaya Shkola, 2000).
42. Schunemann P. *Laser Focus World*, **54** (4), 37 (April 2018).